Photochemical synthesis of a "cage" compound in a microreactor: Rigorous comparison with a batch photoreactor

Tristan Aillet [a,b], Karine Loubiere [a,b,*], Odile Dechy-Cabaret [a,c], Laurent Prat [a,b]

[a] *Université de Toulouse, INPT, ENSIACET, 4 allée Emile Monso, BP 84234, F-31432 Toulouse, France*
[b] *CNRS, Laboratoire de Génie Chimique (LGC UMR 5503), F-31432 Toulouse, France*
[c] *CNRS, Laboratoire de Chimie de Coordination (LCC UPR 8241), 205 route de Narbonne, F-31077 Toulouse, France*

ABSTRACT

An intramolecular [2+2] photocycloaddition is performed in a microphotoreactor (0.81 mL) built by winding FEP tubing around a commercially available Pyrex immersion well in which a medium pressure mercury lamp is inserted. A rigorous comparison with a batch photoreactor (225 mL) is proposed by means of a simple model coupling the reaction kinetics with the mass, momentum and radiative transfer equations. This serves as a basis to explain why the chemical conversion and the irradiation time are respectively increased and reduced in the microphotoreactor relative to those in the batch photoreactor. Through this simple model reaction, some criteria for transposing photochemical synthesis from a batch photoreactor to a continuous microphotoreactor are defined.

1. Introduction

Photochemistry concerns the physical and chemical processes triggered by the absorption of photons. Photochemical reactions are thus based on the use of light (ultra-violet, visible light or sunlight) to provide the activation energy to induce synthesis of a targeted molecule. When absorbing light, molecules reach an electronically excited state, where their electronic and nuclear configurations are different from those in ground state (from a fundamental point of view, these electronic transitions can be described by means of ground-state and excited-state potential-energy hypersurface topology [1]). This induces major changes in the chemical properties of the molecules (in particular reactivity), and offers then a broadened spectrum of possible reaction schemes. In many cases, using photochemistry allows synthesis routes to be shortened, and polycyclic or highly functionalized structures to be obtained, and/or makes new product families available that are difficult to achieve with usual routes (e.g. by heating or using high activity reagents) [2]. For these reasons, synthetic organic photochemistry is an extremely powerful method for the conversion of simple substrates into complex products, opening new perspectives, in particular for the pharmaceutical industry [3]. As the photochemical substrate activation often occurs without additional reagents, the formation of by-products is also minimized, making photochemistry even more attractive in the modern context of Green Chemistry. Some of the main applications of photochemistry are photopolymerization, photohalogenation, photosulfochlorination, photonitrosation, photooxygenation or photocycloaddition [2,3]. These photochemical reactions are commonly performed either in batch reactors irradiated from within or in systems including external irradiation using multiple lamps (Rayonet-type apparatus) and falling film reactors [1]. Despite some impressive large-scale industrial applications (e.g. caprolactam synthesis for nylon production, vitamin D synthesis), the industrial use of photochemistry is still limited by concerns about scalability of light sources, efficiency (low selectivity, reactive intermediate compounds) and the safety of operations (explosions caused by excess heat). The major cause of that is connected with the introduction and the control of adequate illumination.

In the last decade, microreaction technology has been successfully developed, using the features proper to the microspace (small amounts of fluid, short molecular diffusion distance, intensified heat and mass transfers, safety) to improve reaction selectivity and yield, particularly where by-products form due to reaction hot-spots [4]. For photochemistry, microreactors offer additional advantages, namely higher spatial illumination homogeneity and better light penetration throughout the entire reactor depth than in large-scale reactors. Surprisingly, photochemical synthesis in microreactors is rarely encountered in the literature, whereas

microreaction systems have been examined successfully in a wide range of applications of analytical and organic chemistry. Most of these works deal with organic synthesis photoreactions where supported catalysts are involved (titania coated chips) [5–7] and, as yet, little research is concerned with photochemical reactions without supported catalysts [8–15]. The known advantages of microreactors for photochemistry are mainly the enhancement of the chemical conversion and selectivity, and the reduction of the irradiation time [16,17]. At present, there are no reports of attempts to understand and model such results from a classical chemical engineering approach in which reaction kinetics and conservation equations (mass, momentum, thermal energy and radiative transfer) are coupled. For example, an interesting comparison between a batch Rayonet reactor and various microreactors has been proposed recently by Shvydkiv et al. [18]. The criteria used concern conversion rates (space time yield), reactor geometry (illuminated area and volume) and lamp power per illuminated area, but no modeling is proposed.

In keeping with this scientific context, this paper presents an application of microreactors for photochemistry. The synthesis of pentacyclo[5.4.0.0^{2,6}.0^{3,10}.0^{5,9}]undecane-8,11-dione by an intramolecular [2 + 2] photocycloaddition was chosen as the model reaction since this pentacyclic 'cage' compound can be of therapeutic interest [19–21]. Moreover, this reaction offers the advantage of having a simple kinetic scheme as the photochemical excitation of the reactant leads to a single non-absorbing product.

The objectives of this work were, firstly, to quantify the benefits of microreactors for performing this photochemical reaction (especially when compared to a conventional batch photoreactor) and, secondly, to identify the parameters required for comparing photoreactor performance and for transposing photochemical reactions from batch to continuous reactors. For this purpose, experiments were conducted in a microphotoreactor and in a batch photoreactor. For each system, the conversion into the cage compound was measured as a function of irradiation times and reagent concentrations. Based on radiation transfer and mass balances, a model is proposed and some criteria for reactor comparison are defined.

2. Materials and methods

2.1. Photochemical reaction and analytical methods

As described in Fig. 1, the photochemical reaction under test was the synthesis of pentacyclo[5.4.0.0^{2,6}.0^{3,10}.0^{5,9}]undecane-8,11-dione **2** (the 'cage' compound) via the intramolecular [2 + 2]-photocycloaddition of 1,4,4a,8a-tetrahydro-endo-1,4-methanonaphthalene-5,8-dione **1**. Reagent **1** was either prepared through a Diels–Alder reaction involving cyclopentadiene and 1,4-benzoquinone [22], or purchased directly (CAS: 51175-59-8).

The reagent solution could be formulated from the Diels–Alder compound (174.2 g mol^{-1}) diluted in ethyl acetate. The maximum absorption of the resulting solutions occurred between 365 and 372 nm, as shown in Fig. 2a. At 365 nm, the molar absorptivity of reagent **1** (ε_1) was determined using a spectrophotometer (Ultraspec 1000 Pharmacia Biotech®), and found to be

$$\varepsilon_1 = 61.81 \text{ L mol}^{-1} \text{ cm}^{-1} \tag{1}$$

This parameter is in good agreement with the molar extinction coefficients found in the literature for electronic transitions $S_0 \rightarrow S_1$ of the $n \rightarrow \pi^*$ type [1]. In addition, it is interesting to note that no absorption of the cage compound **2** was observed at 365 nm (Fig. 2b).

During the photochemical reaction (i.e. at different irradiation times), samples (0.8 mL in the microreactor, 4 mL in the batch reactor) were taken and stored in the dark in a refrigerator. Then, the solvent was removed under reduced pressure and conversion was calculated by ^{1}H NMR in CDCl$_3$.

2.2. Description of the microphotoreactor and batch photoreactor

As illustrated in Fig. 3a, the microreactor implemented for photochemistry was constructed by winding tubing (508 μm inner diameter, 1587.5 μm outer diameter, 4 m length) in a single pass around a commercially available immersion well made of Pyrex (50 mm outer diameter, 200 mm length). Fluorinated Ethylene Propylene (FEP) was chosen as the tubing material because it is very versatile, solvent resistant and has excellent UV-transmission properties [23]. Tubing was fixed to the well using sticky tape and was covered by aluminum foil to prevent the escape of UV radiation.

Aluminum foil was also used to protect the supply syringe and the inlet and outlet sections of the tubing from UV light, thus ensuring that the photochemical reaction took place only in the tubing section wound around the well, and that the irradiation time (t_{irrad}) could be assumed equal to the residence time (t_S) in this wound section (4 m long). The solution to be irradiated was fed into the reactor tubing by a syringe pump (PHD 2000 Harvard). At the exit of the tubing, samples were collected after a steady state had been reached (three times the residence time). The flow rate (Q)
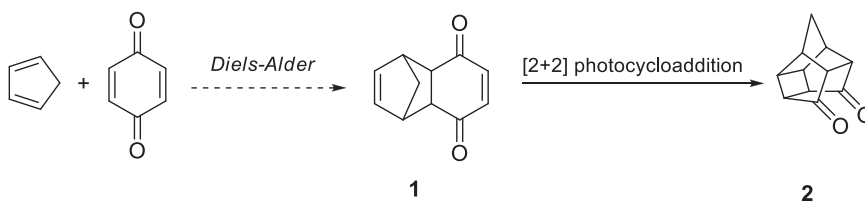
Fig. 1. Photochemical reaction under test (synthesis of a cage compound via an intramolecular [2 + 2]-photocycloaddition).
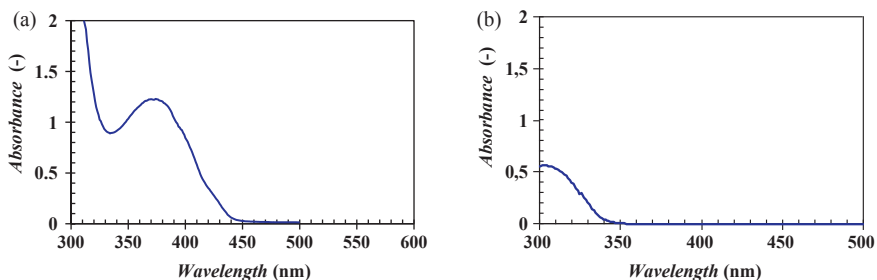
Fig. 2. Absorption spectrum with an optical depth of 10 mm of (a) the 1,4,4a,8a-tetrahydro-endo-1,4-methanonaphthalene-5,8-dione compound (1) in an ethyl acetate solution ($C_{A_0} = 0.02$ mol L^{-1}), and (b) the 'cage' compound (2) in an ethyl acetate solution ($C_{A_0} = 0.02$ mol L^{-1}).

varied between 0.8 and 98 mL h^{-1}, thus covering a range of irradiation times from 30 s to 1 h defined according to:

$$t_{irrad} = t_S = \frac{V_r}{Q} \tag{2}$$

where V_r is the volume in the wound tubing section (0.81 mL). Considering ethyl acetate as the liquid phase ($\rho = 894$ kg m^{-3}, $\mu = 0.552$ mPa s), the corresponding Reynolds numbers varied from 1.8 to 116.

The lamp was inserted inside the well, which was equipped with a double jacket connected to an external cooling unit and a refrigerating water circulator. The temperature was not measured directly inside the microphotoreactor: only the stability of the temperature (8 °C) of the cooling water circulating in the double jacket was checked, assuming that such a device thermally isolated the reaction mixture from the heating lamp.

The lamp was a mercury vapor discharge lamp (medium pressure Hg Ba/Sr lamp, 125 W, HPK Heraeus®) having the dominant emission line at 366 nm, corresponding to the wavelength domain where the absorption of the reactant solution was maximum (Fig. 2a).

For comparison, the photochemical reaction under test was also operated in a conventional batch photoreactor (Fig. 3b) having the same immersion well as the one used for the microphotoreactor.

Fig. 3. (a) Lab-made microphotoreactor and (b) Batch immersion well photoreactor.

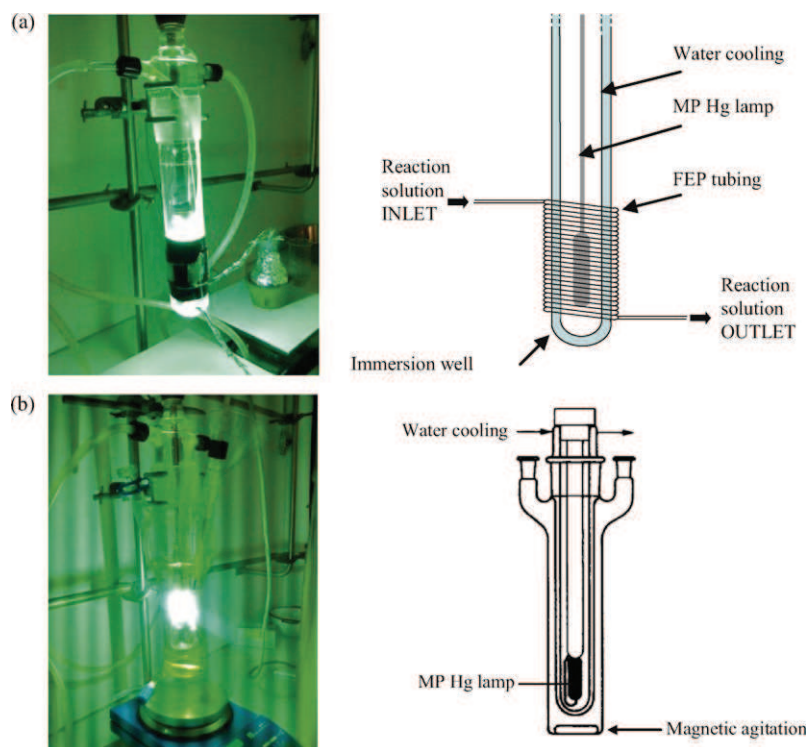| Parameters	Batch reactor	Microreactor
Depth of light penetration (cm)	0.62	0.0508
Irradiated area[a] (cm^2)	300	16
Irradiated volume (cm^3)	225	0.81
Irradiated area/volume ratio ($m^2\,m^{-3}$)	1.33	19.75

[a] Calculated considering a reactor with annular geometry (see Fig. 5): $S_{irrad} = V_r/\Delta s$ where Δs is calculated with Eq. (24).

Table 2
Photochemical reaction steps and associated kinetic rate.

Reaction steps	Kinetic rate
Activation step: $A \xrightarrow{h\nu} A^*$	$r_\lambda^* = (LVRPA)_{\lambda,A}$
Deactivation step: $A^* \to A$	$r_d = k_d \cdot C_{A^*}$
Reaction: $A^* \to B$	$r_B = k_r \cdot C_{A^*}$

The volume of the irradiated solution, V_r, was 225 mL here (against 0.81 mL for the microreactor). The depth of the irradiated solution was 6.2 mm for the batch reactor (annular space between the immersion well outer wall and the inner reactor wall) whereas it was 508 μm in the microreactor (tubing inner diameter). The main technical characteristics of the reactors are listed in Table 1.

3. Theoretical considerations

3.1. Reaction kinetics and mass balance

When dealing with photochemical reactions, it is first necessary to evaluate the rate of the radiation activation step.

The mechanism of the present photochemical reaction was three-step kinetics in homogenous phase, as schematically described in Table 2. A represents the non-excited reagent **1**, A^* reagent **1** in the electronically excited state and B the single reaction product **2**, which is a non-absorbing species (at 365 nm).

In the activation step, the activated molecule A^* was produced by photon absorption; the associated rate was thus directly proportional to the radiant energy absorbed in the reactor per unit of volume. This "useful" energy has been called the local volumetric rate of radiant energy absorption (*LVREA* in $W\,m^{-3}$) [24], or, preferably, the local volumetric rate of photon absorption (*LVRPA* in mol-photon m^{-3} or in einstein m^{-3}). Defined at a given wavelength λ and for a given species A, these two parameters are linked according to:

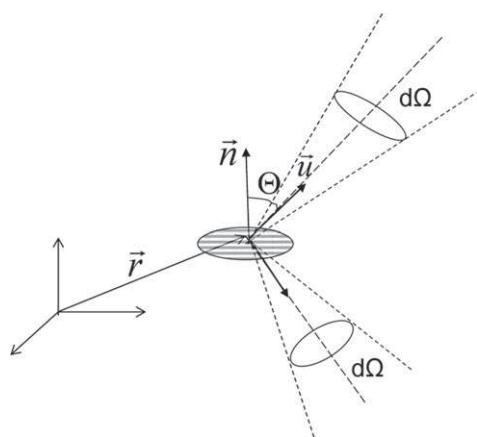$$(LVRPA)_{\lambda,A} = \frac{1}{N_a} \cdot \frac{h \cdot c}{\lambda} \cdot (LVREA)_{\lambda,A} \tag{3}$$

Fig. 4. General parameters used to define the radiation field.

where h is the Planck constant (6.6256×10^{-34} J s photon^{-1}), c the speed of light (2.9979×10^8 m s^{-1}) and N_a the Avogadro number (6.023×10^{23} mol^{-1}).

Once produced, the activated species A^* either gave the compound B (reaction step) or disappeared (deactivation step). For the reaction under test, the deactivation step corresponded only to a return of the molecule to the ground state by radiative (phosphorescence, fluorescence) or non-radiative deactivation mechanisms. Note that, in a more general case, additional deactivation mechanisms may also exist, in particular the ones resulting from the transformation of radical intermediates. In this case, the equation for deactivation reported in Table 2 is the sum of different processes.

The net balance for the intermediate molecule A^* can be expressed as:

$$\frac{dC_{A^*}}{dt} = r_\lambda^* - r_d - r_B \tag{4}$$

As the life-time of the excited state is very short and the source of light energy is continuous and moderate, the assumption of the quasi-steady state for the intermediate molecule A^* can be applied:

$$\frac{dC_{A^*}}{dt} \approx 0 \tag{5}$$

Thus, the rate of formation of B is linked to the rate of consumption of $A (r_A = -r_\lambda^*)$, such that:

$$r_{A,\lambda} = -r_{B,\lambda} = -k_r \cdot C_{A^*} = -k_r \cdot \frac{(LVRPA)_{\lambda,A}}{k_d + k_r} = \phi_\lambda \cdot (LVRPA)_{\lambda,A} \tag{6}$$

ϕ_λ is the quantum yield of the reaction, defined as the ratio between the rate of molar production of B and the rate of photon molar absorption:

$$\phi_\lambda = \frac{r_B}{r_\lambda^*} = \frac{k_r}{k_d + k_r} \tag{7}$$

where k_r and k_d are the kinetic constants of the photochemical reaction and of the deactivation reaction respectively. Eqs. (6) and (7) show that the quantum yield and the *LVRPA* depend on the wavelength considered, implying that the rate of recovery of A should be rigorously defined for each wavelength.

The complete modeling of a conventional chemical reactor requires the momentum, thermal energy and mass conservation equations to be solved together with the kinetics equations. In the case of a photoreactor, the radiation equation must be added [24].

In the present study, some simplifications can be made based on the following assumptions. Firstly, the energy balance can be neglected. Various experiments performed at different temperatures (from 8 °C to 40 °C) have suggested that the photochemical reaction under test is not temperature sensitive. In addition, all the experiments were performed at a fixed, controlled temperature (close to 20 °C).

Secondly, the mass balance in the case of photochemistry is directly coupled with the radiation equation by means of the reaction rate term (Eq. (6)). The consequence is that a heterogeneous field of concentration is inevitably generated inside the reactor due to photon absorption by the species present. Nevertheless, this spatial non-uniformity of concentrations can be attenuated in presence of good mixing conditions [24]. When the reactant A is the single absorbing species, the impact on this non-uniformity is also reduced because of the change of the radiation field with the chemical conversion. The first absorbing zones (i.e. the ones close to the optical face of the reactor) become clearer (less absorbing) as the conversion increases, allowing light to penetrate farther into the depth of the reactor. In this study, two model cases will be considered:
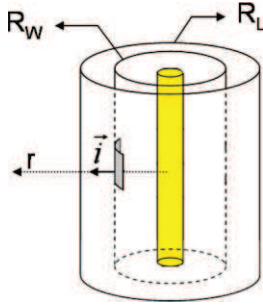
Fig. 5. Specific parameters used to define the radiation field in the batch photore-actor and in the microphotoreactor.

- For the batch photoreactor, perfectly mixed behavior with a constant volume.
- For the microphotoreactor, plug flow behavior.

Under these assumptions, it can be demonstrated that the following equation can be applied for the compound A in the batch reactor:

$$< r_{A,\lambda} > = \frac{dC_A}{dt} = -\phi_\lambda \cdot < LVRPA_{\lambda,A} > \tag{8}$$

where the concentration C_A of compound A is a function of time t in the batch photoreactor (as spatial homogeneity in the whole reactor volume is assumed), and $< LVRPA_{\lambda,A} >$ is the local volumetric rate of photon absorption due to reagent A averaged over the whole volume of the batch photoreactor.

It is interesting to observe that, in the microphotoreactor, in which plug flow behavior is considered, an equation identical to Eq. (8) can be obtained by replacing the axial position x by time, t, according to:

$$dt = \frac{dx}{U} \tag{9}$$

where U is the mean velocity of the reactant solution in the microreactor tube.

3.2. Radiation field inside the photoreactor

3.2.1. Definitions

Let us recall a few definitions. The basic quantity is the monochromatic radiant energy flux density vector [25,26]:

$$\vec{q}_\lambda = \int_{4\pi} L_\lambda(\vec{r}, \vec{u}) \cdot \vec{u} \cdot d\Omega \tag{10}$$

where $\vec{u}$ is the unit vector related to the direction of radiation propagation, $\vec{r}$ the position vector, and $d\Omega$ the solid angle element around the propagation direction $\vec{u}$ (Fig. 4). L_λ is the specific intensity, which represents the radiative energy flow per unit of time, unit

of solid angle and unit of surface normal to the propagation direction. In the literature, it is also called radiance or luminance, and is sometimes noted I_λ instead of L_λ.

Hence, the dot product of $\vec{q}_\lambda$ and $\vec{n}$ (the unit vector normal to receptor surface) gives the net radiative energy flux density passing through the surface of direction $\vec{n}$, which is expressed in watts per unit of receptor surface:

$$q_\lambda = \int_{4\pi} L_\lambda(\vec{r}, \vec{u}) \cdot \vec{u} \cdot d\Omega \cdot \vec{n} = \int_{4\pi} L_\lambda(\vec{r}, \vec{u}) \cdot \vec{u} \cdot \vec{n} \cdot d\Omega$$

$$= \int_{4\pi} L_\lambda(\vec{r}, \vec{u}) \cdot \cos\Theta \cdot d\Omega \tag{11}$$

where Θ is the angle between $\vec{u}$ and the normal $\vec{n}$ to the surface considered (Fig. 4).

We also define the monochromatic spherical irradiance (or scalar irradiance) as the integral over all the directions of the specific intensity L_λ

$$G_\lambda(\vec{r}) = \int_{4\pi} L_\lambda(\vec{r}, \vec{u}) \cdot d\Omega \tag{12}$$

This physical quantity plays an important role in photochemistry as, in an element of reactor volume, the monochromatic radiant energy absorbed by a component j is given by:

$$LVREA_{\lambda,j} = \kappa_{\lambda,j} \cdot G_\lambda(r) \tag{13}$$

where $\kappa_{\lambda,j}$ is the absorption coefficient of the radiation due to the species j.

3.2.2. Radiation balance in a fixed control volume

For a homogeneous and non-emitting medium in which the radiation attenuation is due only to absorption by the medium (i.e. no or negligible scattering effects), the radiative transfer equation (RTE) is written as [24,27,28]:

$$\vec{u} \cdot \overrightarrow{grad}(L_\lambda) = -\kappa_\lambda \cdot L_\lambda \tag{14}$$

Note that, in this form, the RTE is equivalent to the well known Lambert's law.

The integration of the simplified RTE (Eq. (14)) over all solid angles Ω leads to the following general form of the local radiation balance for a non-emitting, homogeneous control volume [27,29]:

$$div(\vec{q}_\lambda) = -\kappa_\lambda \cdot G_\lambda = LVREA_\lambda \tag{15}$$

3.2.3. Expression of the average volumetric rate of photon absorption <LVRPA>

In the following, we have chosen to reduce the problem to a one-dimensional annular cylindrical system (the angular and axial symmetry conditions are verified in both reactors) with radiation in a single direction and normal to the wall surface (Fig. 5). With this
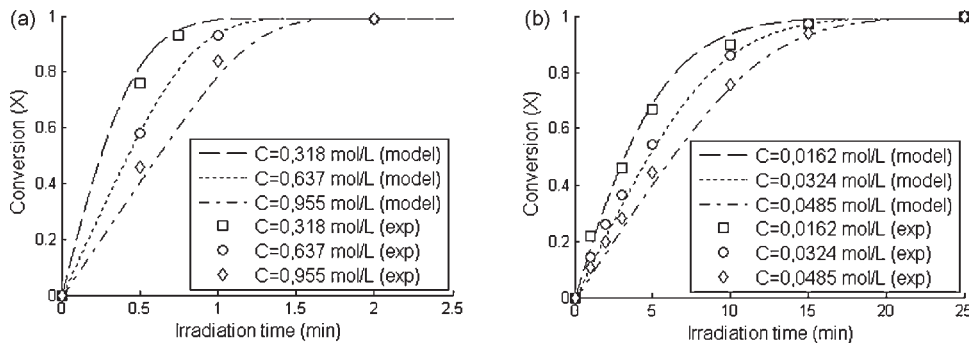

Fig. 6. Conversion into the cage compound versus irradiation time (a) for the microphotoreactor and (b) for the batch photoreactor (in the key, C corresponds to C_{A_0}).

convenient simplification, a mathematical solution for expressing *LVRPA* can be developed, as shown below.

The above assumptions can be written mathematically as:

$$L_\lambda(\vec{r}, \vec{u}) = \bar{L}_\lambda(r) \cdot \delta(\vec{u} - \vec{i}) \tag{16}$$

where $\vec{i}$ is the unit vector related to the single direction that coincides with the radial axis. $\bar{L}_\lambda(r)$, the specific monochromatic intensity defined at a given position r and averaged over all the directions of radiation propagation ($\bar{L}_\lambda(r)$ is thus expressed in watts per surface unit) and δ the Dirac function (in sr^{-1}) is defined as:

$$\delta = \begin{cases} \int_\Omega \delta(\vec{u} - \vec{i}) d\Omega = 1 & \text{if } \vec{u} = \vec{i} \\ \delta(\vec{u} - \vec{i}) = 0 & \text{if } \vec{u} \neq \vec{i} \end{cases} \tag{17}$$

When this expression for L_v (Eq. (16)) is put into the expressions for the net radiation flux and the spherical irradiance (Eqs. (11)–(12)), Eq. (15) becomes (in the case of a one-dimensional cylindrical coordinate system with single-directional radiation):

$$\frac{\partial(r \cdot \bar{G}_\lambda(r))}{r \cdot \partial r} = \frac{\partial(r \cdot \bar{q}_\lambda(r))}{r \cdot \partial r} = -\kappa_\lambda \cdot \bar{G}_\lambda(r) \tag{18}$$

where $\bar{q}_\lambda(r) = \bar{G}_\lambda(r)$ (the direction of light emission is assumed normal to the receptor surface of the reactor). This equation is also well-known as the radial model [25,30].

κ_λ is the absorption coefficient of the reacting mixture (including reagents and products) and is considered to be a linear function of the concentration of the absorbing species. Thus [24,30]:

$$\kappa_{\lambda,j} = \alpha_{\lambda,j} \cdot C_j \tag{19}$$

where $\alpha_{\lambda,j}$ is the molar Napierian absorptivity of the radiation-absorbing species j at a given wavelength λ, and C_j is the molar concentration of the species j. Note that chemists generally use the molar absorptivity $\varepsilon_{\lambda,j}$ defined as:

$$\alpha_{\lambda,j} = 2.303 \cdot \varepsilon_{\lambda,j} \tag{20}$$

When several species absorb radiation in the system and when moderate concentrations are involved, the assumption of absorption additivity can be applied according to:

$$\kappa_\lambda = \sum_j \alpha_{\lambda,j} \cdot C_j = \sum_j \kappa_{\lambda,j} \tag{21}$$

As the concentration C_j changes with the chemical conversion, the *LVREA*$_{\lambda,j}$ will also be dependent on the chemical conversion (Eq. (15)).

The integration of Eq. (18) from the irradiated wall surface of the reactor, R_w (here equal to 25 mm for both reactors, see Fig. 5) to a radial position r inside the reactor leads to:

$$G_\lambda(r) = G_\lambda^W \cdot \frac{R_w}{r} \cdot \exp[(-\kappa_\lambda \cdot (r - R_w))] \tag{22}$$

where G_λ^W is the monochromatic spherical irradiance received at the wall surface of the reactor. Note that Eq. (22) is valid only when the concentration C_j is uniform in the control volume.

The average volumetric rate of energy absorption *<LVREA*$_{\lambda,A}$*>* can be calculated as:

$$< LVREA_{\lambda,A} > = \frac{1}{V} \iiint_V \kappa_{\lambda,A} \cdot G_\lambda(r) \cdot r \cdot dr \cdot d\theta \cdot dz$$

$$= \frac{G_\lambda^W}{\Delta s} \cdot \frac{\kappa_{\lambda,A}}{\kappa_\lambda} \cdot (1 - \exp[-\kappa_\lambda \cdot (R_L - R_w)]) \tag{23}$$

where as shown in Fig. 5, R_L corresponds to the outer radial position of the reactor ($R_W + 0.62$ cm for the batch photoreactor and $R_W + 508$ μm for the microphotoreactor) and Δs is defined by:

$$\Delta s = \frac{R_L^2 - R_W^2}{2R_W} \tag{24}$$

In Eq. (23), G_λ^W is expressed in watts per unit of surface area but can also be converted into einstein per unit of time and per unit of surface area ($G_\lambda^{W,photon}$) by using Eq. (3).

3.3. Coupling between radiation field and mass balance

For the photochemical reaction under test, compound A is the only absorbing species and this leads to:

$$\kappa_{\lambda,A} = \kappa_\lambda = \alpha_A \cdot C_A \quad \text{and} \quad \frac{\kappa_{\lambda,A}}{\kappa_\lambda} = 1 \tag{25}$$

Rigorously speaking, a reaction rate equation (Eq. (6)) may be written for each emitted wavelength at which the compound absorbs, and thus the knowledge of G_λ^W and $\alpha_{\lambda,j}$ may be required for each wavelength concerned. The global rate would then be the sum of all the rate equations. Without loss of accuracy, we will consider a single wavelength, 365 nm, in this study as the reactant mainly absorbs at this wavelength (Fig. 2a) which corresponds to a significant emission ray of the lamp. Consequently, in the following, the index "λ" will no longer be attached to the variables.

The concentration, C_A, of compound A can be expressed as a function of the chemical conversion X:

$$C_A = C_{A_0} \cdot (1 - X) \tag{26}$$

where C_{A_0} is the concentration of the compound A initially introduced into the reactor (at $t = 0$). Finally, the coupling of the mass balance (Eq. (8)) with the expression of the average volumetric rate of photon absorption *<LVRPA>* (Eq. (23)) can be formulated as:

$$C_{A_0} \frac{dX}{dt} = -\phi \cdot \frac{G^{W,photon}}{\Delta s} \cdot (1 - \exp[-B_0 \cdot (1 - X)]) \tag{27}$$

where B_0 is the initial Napierian optical density defined by

$$B_0 = C_{A_0} \cdot \alpha_A \cdot (R_L - R_w) \tag{28}$$

When Eq. (27) is integrated over time, the following expression is obtained:

$$C_{A_0} \cdot \left(X + \frac{1}{B_0} \cdot \ln\left[\frac{1 - \exp(-B_0)}{1 - \exp(-B_0 \cdot (1 - X))} \right] \right) = \phi \cdot \frac{G^{W,photon}}{\Delta s} \cdot t \tag{29}$$

From Eq. (29), it can be shown that complete modeling of the reactor requires the knowledge of the quantum yield ϕ and of the spherical irradiance received at the wall surface of the reactor ($G^{W,photon} \approx G_{365}^{W,photon}$). Generally, this is determined either from the lamp emission model or from experiments (actinometry).

4. Results and discussion

4.1. Variation of conversion with concentration and irradiation time

Firstly, the effect of the initial concentration of the compound A (C_{A_0}) on the conversion of the Diels–Alder compound into the 'cage' compound (X) was investigated as a function of the irradiation times in the microphotoreactor (Fig. 6a). As expected, for a fixed irradiation time, conversion decreased with increasing concentrations. This is consistent with the radiative transfer model previously established (Eq. (22)): for any radial position $R_w < r < R_L$, an increase of C_{A_0} (i.e. of the absorption coefficient κ_A) induces a decrease of the exponential factor and thus a decrease of the spherical irradiance
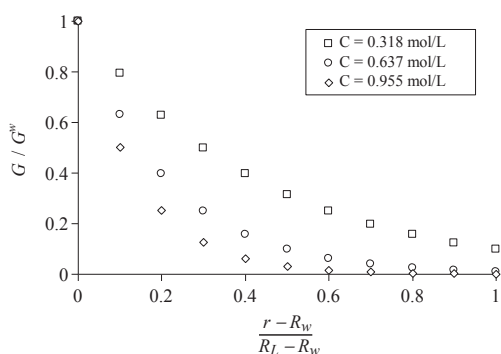
Fig. 7. Initial (namely, at $t = 0$, $X = 0$) light attenuation profiles along the depth of the microphotoreactor (in the key, C corresponds to C_{A_0}).

(G). When considering the initial light attenuation along the reactor depth (deduced from Eq. (22) and represented in Fig. 7), we clearly observed that the light penetration was lower when concentrated solutions were involved, thus reducing the fraction of the volume inside the reactor that was illuminated.

Fig. 6a also shows that, whatever the initial concentration, a few minutes were sufficient to achieve high photochemical conversions. It is particularly interesting to note that the full conversion ($X = 100\%$) was achieved at 1 min for the lowest concentration (0.318 mol L^{-1}) and at 2 min for $C_{A_0} = 0.637$ mol L^{-1} and $C_{A_0} = 0.955$ mol L^{-1}.

These performance levels were compared with those obtained in the batch photoreactor, the latter reactor being the conventional device for photochemistry. The criterion chosen for comparison was the conservation of the same order of magnitude of the initial optical Napierian densities B_0 (and thus of irradiance attenuation profiles inside the solution) in both photoreactors. The light penetration depth ($R_L - R_W$) being dependent on the reactor, the initial concentrations C_{A_0} thus needed to be adjusted (using Eq. (28)) for experiments in the batch photoreactor (Table 3). Note that it was not possible to use more concentrated solutions in the batch photoreactor as they would have induced too high a reactant consumption.

The variation of the conversion with the irradiation time is plotted in Fig. 6b for the batch photoreactor. Here too, for a given irradiation time, more concentrated solutions generated smaller conversions. Whatever the concentrations, a minimum of 30 min irradiation time was required to achieve the full conversion, compared with 1 or 2 min in the microphotoreactor. For comparison purposes, it was interesting to estimate the reactor efficiency by introducing the space-time yield (STY), a parameter commonly used by chemists. It represents the total amount of product (cage compound) per reactor volume per irradiation time, as:

$$STY = \frac{C_{A_0} \cdot X}{t_{irrad}} \tag{30}$$

It was calculated here for a conversion of 90% and an average initial concentration C_{A_0} in each reactor (0.637 mol L^{-1} in the microphotoreactor and 0.0324 mol L^{-1} in the batch

Table 3
Initial concentration of Diels–Alder and associated optical Napierian density in the microphotoreactor and in the batch photoreactor.

Microphotoreactor		Batch photoreactor	
C_{A_0} (mol L^{-1})	B_0	C_{A_0} (mol L^{-1})	B_0
0.319	2.3	0.0162	1.4
0.637	4.6	0.0324	2.9
0.955	6.9	0.0485	4.3

photoreactor). In these conditions, STY was found to be equal to 573 mmol L^{-1} min^{-1} in the microphotoreactor and 2.3 mmol L^{-1} min^{-1} in the batch photoreactor. From this, we can conclude that using a microphotoreactor significantly improved the space-time yields or, in other words, decreased the minimal irradiation time required to achieve complete conversion while working with more concentrated solutions. In agreement with the results already reported in the literature [4–18], this first finding offers promising perspectives for implementing photochemical synthesis in microreactors. Nevertheless, some underlying questions must be addressed: *How can such results be explained? Which criteria should be defined to rigorously compare performance in different photochemical reactors and/or to transpose results from batch to continuous microphotoreactors?*

4.2. Data analysis based on the model coupling reaction kinetics, conservation and radiation transfer equations

4.2.1. Determination of the product $\phi \cdot G^{W,photon}$

In keeping with the questions posed above, a simplified model (Eq. (29)) has previously been proposed to link the radiation transfer balance (1D annular cylindrical system, homogeneous and non-emitting medium, negligible scattering effect, single absorbing species, monochromatic and single-directional light source) and mass balances (three-step kinetics, perfectly mixed, plug flow behavior). The application of this model to the experimental data supposes that the quantum yield of the reaction (ϕ) and the irradiance at the wall surface of the reactor ($G^{W,photon}$) are known. As this was not the case, the product $\phi \cdot G^{W,photon}$ was directly determined by fitting Eq. (29) with experimental measurements. This led to $\phi \cdot G^{W,photon} = 0.029$ einstein s^{-1} m^{-2} for the batch photoreactor and to $\phi \cdot G^{W,photon} = 0.404$ einstein s^{-1} m^{-2} for the microphotoreactor. The ratio of these two quantities was close to 0.07, and was mainly explained by the ratio between the irradiated surfaces in the microreactor and in the batch reactor (Table 1), as shown below:

$$\frac{S_{irrad,microreactor}}{S_{irrad,batch}} = \frac{16}{300} \approx 0.053 \tag{31}$$

The deviation could be attributed to some approximations (calculation of the irradiated surface in the microphotoreactor, reflections neglected and assumption of a monochromatic emission) and/or to a possible change of the quantum yield (the range of concentrations being significantly different in the two photoreactors).

Lastly, it is interesting to note that this modeling describes the variation of experimental conversion with time well, whatever the initial concentration and reactor (Fig. 6).

4.2.2. Definition of some consistent ratios for reactor comparison purposes

To explain the differences observed in terms of irradiation time between the two reactors, let us introduce several supplementary physical parameters.

- The first one is the power P (expressed in einstein s^{-1}) defined according to:

$$P = V_r \cdot \frac{\phi \cdot G^{W,photon}}{\Delta s} \tag{32}$$

It corresponds to the maximum power than can be received in the photoreactor, i.e. when all the photons are absorbed by the reaction mixture (no transmittance). As defined by Eq. (32), this value also integrates the quantum yield of the reaction, which gives the ratio between the rate of molar production of B and the rate of the photon molar absorption. Finally, this

power makes the connection between the light emitted by the lamp and the design of the reactor or, in other words, is an expression of the manner in which the reactor is exposed to the lamp.

- The second parameter of great importance is the photonic efficiency. Noted as, depending η^X on the conversion X, it represents the efficiency of the reactor, that is to say the ratio between the number of moles of compound B produced and the number of moles of photons received:

$$\eta^X = \frac{C_{A_0} \cdot V_r \cdot X}{P \cdot t_{irrad}^X} \tag{33}$$

Expressing t_{irrad} with Eq. (29) and P with Eq. (32), we obtain:

$$\eta^X = \frac{X}{(X + (1/B_0) \cdot \ln[(1 - \exp(-B_0))/(1 - \exp(-B_0 \cdot (1 - X)))])} \tag{34}$$

If $\eta^X \to 1$, all the photons received in the system are used to reach the desired conversion. In contrast, if $\eta^X \to 0$, the efficiency of the reactor is low, meaning that many of the photons received in the reactor are not absorbed (i.e. are transmitted over the outer side of the reactor) because of a low optical density in the reactor. Considering this definition, it is clear that the photoreactor will operate better when high optical density is involved. Varying between 0 and 1, this photonic efficiency must not be confused with the quantum yield, which is a parameter intrinsic to the photochemical mechanism and represents the amount of absorbed photons necessary to convert a given amount of reactant molecules (Eq. (7)). In contrast, the photonic efficiency defined by Equation 34 deals only with the radiation attenuation profile in the medium.

- The third parameter is the productivity, which represents the molar quantity produced per unit of irradiation time and also depends on the conversion X, as:

$$R^X = \frac{C_{A_0} \cdot V_r \cdot X}{t_{irrad}^X} = P \cdot \eta^X$$

$$= P \cdot \frac{X}{(X + (1/B_0) \cdot \ln[1 - \exp(-B_0)/1 - \exp(-B_0 \cdot (1 - X))])} \tag{35}$$

- It is also interesting to describe the space-time yield (STY) previously introduced (Eq. (30)) as follows:

$$STY^X = \frac{C_{A_0} \cdot X}{t_{irrad}^X} = \frac{P}{V_r} \eta^X$$

$$= \frac{P}{V_r} \cdot \frac{X}{(X + (1/B_0) \cdot \ln[(1 - \exp(-B_0))/(1 - \exp(-B_0 \cdot (1 - X)))])} \tag{36}$$

To compare the performance in the two reactors, five criteria are defined, corresponding to the ratios between the power received, the photonic efficiency, the productivity, the irradiation time, and the space-time yield in the microreactor and in the batch reactor. They are brought together in Table 4.

From Table 4, we can observe that:

- the ratios related to the power received and to the photonic efficiency are the ones governing the others, as $\chi_R^X = f(\chi_P, \chi_\eta^X)$, $\chi_t^X = g(\chi_P, \chi_\eta^X)$ and $\chi_{STY}^X = h(\chi_P, \chi_\eta^X)$,
- the power ratio χ_P lets us compare the exposure to the light source in the two photoreactors and depends directly on the geometry of the photoreactors. If $\chi_P \to 1$, the photoreactors are exposed to the same total amount of radiant energy,
- the photonic efficiency χ_η^X compares, for a given conversion, the radiation field in the two photoreactors. If $\chi_\eta^X \to 1$, the irradiance attenuation along the reactor depth is the same in both photoreactors.

4.2.3. Comparison of the two reactors based on the calculations of the previous ratios

All the parameters involved in Eq. (32) being known, the power ratio, χ_P, can be calculated. It is found to be 0.73, meaning that the microphotoreactor as designed in the present experiments receives fewer photons than the batch reactor. This result is not surprising because the tubing constituting the microphotoreactor was wound around the straight section of the immersion well, and only over a few centimeters in height (Fig. 3a) whereas, for the batch photoreactor, the solution volume was also located under and on top of the lamp (Fig. 3b). Moreover, because of the tubing curvature, some of the rays could be reflected. The important idea to note is that this ratio can be easily improved by winding the tubing around the entire height of the immersion well as already done by Hook et al. [13].

Concerning the photonic efficiency ratio χ_η^X, Fig. 8 presents the iso-curves of this ratio for a conversion of 90%, and their change with the initial Napierian optical densities (B_0) in each photoreactor. It is convenient to define three main areas on this graph:

- Area A: the photonic efficiency in the batch photoreactor is better here ($\chi_\eta^{0.90} < 1$). In other words, the fraction of "wasted" photons (i.e. transmitted outside the reactor) is lower in the batch photoreactor than in the microphotoreactor, due to a higher optical density.
- Area C: this is the opposite of area A.
- Area B: this area corresponds to the part of Fig. 8 between the iso-curves 1.05 and 0.95, implying that the efficiencies in the reactors are approximately the same ($|(\eta_{microreactor} - \eta_{batch})/$

Table 4
Ratio defined to compare the microphotoreactor and batch photoreactor.

Ratio of	Definitions
Power received P	$\chi_P = \frac{P_{microreactor}}{P_{batch}}$
Photonic efficiency η^X	$\chi_\eta^X = \frac{\eta_{microreactor}^X}{\eta_{batch}^X} = \frac{F_{batch}^X}{F_{microreactor}^X}$
Productivity R^X	$\chi_R^X = \frac{R_{microreactor}^X}{R_{batch}^X} = \chi_P \cdot \chi_\eta^X$
Irradiation time t^X	$\chi_t^X = \frac{t_{microreactor}^X}{t_{batch}^X} = \frac{1}{\chi_\eta^X \cdot \chi_P} \cdot \frac{V_{r,micro}}{V_{r,batch}} \cdot \frac{C_{A_0,micro}}{C_{A_0,batch}}$
Space-time yield (STY)	$\chi_{STY}^X = \chi_P \cdot \chi_\eta^X \cdot \frac{V_{r,batch}}{V_{r,micro}}$

With $F_{microreactor}^X = \left(X + \frac{1}{B_{0,micro}} \ln\left[\frac{1-\exp(-B_{0,micro})}{1-\exp(-B_{0,micro} \cdot (1-X))}\right]\right)$ $F_{batch}^X = \left(X + \frac{1}{B_{0,batch}} \ln\left[\frac{1-\exp(-B_{0,batch})}{1-\exp(-B_{0,batch} \cdot (1-X))}\right]\right)$
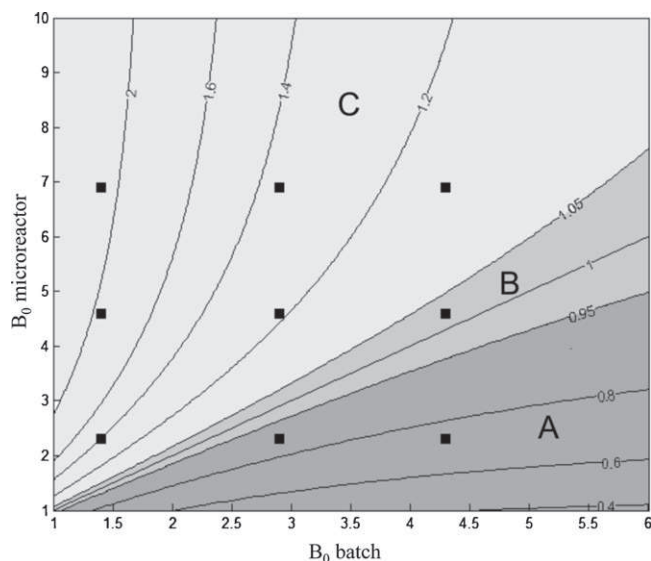
Fig. 8. Iso-curves of the photonic efficiency ratio to reach a conversion of 90% ($\chi_\eta^{0,90}$). The black square symbols correspond to experimental photonic efficiency ratios.

$\eta_{batch}| < 0.05$). In this case, the fraction of "wasted" photons is equivalent in both photoreactors (the light attenuation profiles remain identical whatever the conversion).

The experimental efficiency ratios are also reported in Fig. 8 (black squares). It can be observed that, depending on the initial optical density, the different areas are covered by the experimental conditions.

Concerning the productivity ratio χ_R^X, they can be either calculated using the product $\chi_P \cdot \chi_\eta^X$ (Table 4) or estimated from experimental data as:

$$\chi_R^{0.9} = \frac{(C_{A0} \cdot V_r \cdot 0.9/t_{irrad}^{0.9})_{micro}}{(C_{A0} \cdot V_r \cdot 0.9/t_{irrad}^{0.9})_{batch}} \tag{37}$$

Table 5 reports the calculated and experimental (in brackets) productivity ratios. It is clear that the initial optical density (B_0) has a drastic impact on the productivity ratio value. This latter parameter B_0 is thus the key parameter to maintain constant when transposing a photochemical synthesis from a batch reactor to a continuous (micro)reactor.

It is important to keep in mind that this finding is true only because the photochemical reaction scheme under test is $A \to B$ with a single absorbing species A. For more complex reactions (in particular when there are several strongly absorbing species in the medium), it will be necessary to account for the role of hydrodynamics (mixing) on the spatial and time distributions of the active species in the different light level areas existing in the reactor. For this, the present model may be extended by considering, in the previous equations, the absorption coefficient of each species, the two-(or three-) dimensional character of the flow, and the complete reactional scheme.

Table 5
Experimental and calculated (in brackets) productivity ratios.

	$B_{0\,batch}$		
	1.43	2.85	4.28
$B_{0\,microreactor}$			
2.29	0.9 (1.0)	0.56 (0.64)	0.45 (0.54)
4.6	1.5 (1.39)	0.83 (0.90)	0.68 (0.75)
6.90	1.73 (1.99)	0.98 (1.17)	0.82 (0.91)

Regarding the irradiation time ratio $\chi_t^{0.9}$ (at a conversion X of 90%), the experimental ratios (deduced from Fig. 6) are found to vary between 0.044 and 0.1. Such a finding can be directly explained by the model proposed, in which $\chi_t^{0.9}$ depends on χ_P, $\chi_\eta^{0.9}$, reactor volumes and initial concentrations. Let us consider a power ratio χ_P of 0.73 and a representative photonic efficiency $\chi_\eta^{0.9}$ of 1 (implying identical initial optical density). The time ratio is then expressed as (Table 4):

$$\begin{aligned}\chi_t^X &= \frac{1}{1 \times 0.73} \cdot \frac{V_{r,micro}}{V_{r,batch}} \cdot \frac{C_{A_0,micro}}{C_{A_0,batch}}\\ &= \frac{1}{1 \times 0.73} \cdot \frac{V_{r,micro}}{V_{r,batch}} \cdot \frac{\alpha_A \cdot (R_L - R_W)_{batch}}{\alpha_A \cdot (R_L - R_W)_{micro}}\end{aligned} \tag{38}$$

Considering the geometrical characteristics of the two reactors, $\chi_t^{0.9}$ is found to be equal to 0.06, which is in perfect agreement with the experimental time ratios. This demonstrates that the improvement in irradiation times previously observed in the microphotoreactor was mainly due to the difference in the number of absorbing molecules ($V_r \times C_{A_0}$).

It is interesting to observe that the values of the *STY* ratios, χ_{STY}^X, are mainly controlled by the reactor volume ratios. Again, if a power ratio χ_P of 0.73 and a representative photonic efficiency $\chi_\eta^{0.9}$ of 1 are assumed, Eq. (36) leads to $\chi_{STY}^X \approx 200$, which agrees perfectly with the experimental values discussed in Section 4.1.

4.3. Synthesis and first conclusions

From the simple model proposed, two main criteria have been identified for designing and comparing photoreactors: the power received in the system (P) and the photonic efficiency (η^X). These two parameters should be equal if equivalent productivity is to be obtained in both photoreactors, the photonic efficiency being the parameter of interest from an industrial point of view.

Finally, from these findings, some suggestions can be made for improving performance in the microphotoreactor:

- the tube length wound around the immersion well can easily be increased so as to receive maximum radiation from the source. In this way, the power received in the microphotoreactor can be larger than in a conventional batch immersion photoreactor ($\chi_P > 1$);
- keeping the photonic efficiency identical in both reactors implies working with higher concentrations in the microphotoreactor (smaller optical length). As it can induce some limitations in terms of compound solubility in the solvent, the number of tubing passes around the immersion well can be increased or a slightly larger inner diameter of tubing used.

5. Conclusion

In conclusion, the simple and easy-to-construct microphotoreactor proposed can ensure the continuous photochemical synthesis of a pentacyclic 'cage' compound, and reach full conversion of highly concentrated solution in a short irradiation time. In this study, a comparison has been made between the microphotoreactor and a conventional batch photoreactor by introducing a simplified model combining reaction kinetics, conservation and radiative transfer equations. This study points out that two main criteria are essential for designing and comparing photoreactors: the power received in the system (P) and the photonic efficiency (η^X). Keeping these two criteria constant in both photoreactors will inevitably lead to equivalent productivity. The approach presented in this paper is only valid for the case of an $A \to B$ reaction scheme,

with a single absorbing species *A*. The mixing effect is thus reduced, enabling some simplifications to be used.

A specific research effort should be made in the future to propose a more complex model able to take account of the impact of the short diffusion distances in the microphotoreactor when several species are absorbing in the medium. In these cases, the effect of mixing becomes a critical parameter to ensure efficient spatial and time distributions of the active species in the different light level areas existing in the reactor.

References

[1] A.M. Braun, M.-T. Maurette, E. Oliveros, Technologie photochimique, Presses Polytechniques Romandes, 1986.

[2] K.-H. Pfoertner, B. Swirtzerland, Photochemistry Ullmann's Encyclopedia of Industrial Chemistry, Wiley-VCH Verlag GmbH & Co. KGaA, Weinheim, 2005.

[3] N. Hoffmann, Photochemical reactions as key steps in organic synthesis, Chemical Reviews 108 (2008) 1052.

[4] T.R. Dietrich, Microchemical engineering in practice, in: Photoreactions, Wiley, 2009 (Chapter 17).

[5] Y. Matsushita, T. Ichimura, N. Ohba, S. Kumada, K. Sakeda, T. Suzuki, H. Tanibata, T. Murata, Recent progress on photoreactions in microreactors, Pure and Applied Chemistry 79 (11) (2007) 1959–1968.

[6] Y. Matsushita, S. Kumada, K. Wakabayashi, K. Sakada, T. Ichimura, Photocatalytic reduction in microreactors, Chemistry Letters 35 (410) (2006).

[7] R. Gorges, S. Meyer, G. Kreisel, Photocatalysis in microreactors, Journal of Photochemistry and Photobiology A-Chemistry 167 (95) (2004).

[8] H. Lu, M.A. Schmidt, K.F. Jensen, Photochemical reactions and on-line UV detection in microfabricated reactors, Lab Chip 1 (2001) 22–28.

[9] K. Ueno, F. Kitagawa, N. Kitamura, Photocyanation of pyrene across an oil/water interface in a polymer microchannel chip, Lab Chip 2 (2002) 231–234.

[10] H. Maeda, H. Mukae, K. Mizuno, Enhanced efficiency and regioselectivity of intramolecular $(2\pi + 2\pi)$ photocycloaddition of 1-cyanonaphtalene derivative using microreactors, Chemistry Letters 34 (66) (2005).

[11] T. Fukuyama, Y. Hino, N. Kamata, I. Ryu, Quick execution of [2 + 2] type photochemical cycloaddition reaction by continuous flow system using a glass-made microreactor, Chemistry Letters 33 (11) (2004) 1430–1431.

[12] A. Vasudevan, C. Villamil, J. Trumbull, J. Olson, D. Sutherland, J. Pan, S. Djuric, LOPHTOR: a convenient flow-based photochemical reactor, Tetrahedron Letters 51 (31) (2010) 4007–4009.

[13] B.D.A. Hook, W. Dohle, P.R. Hirst, M. Pickworth, M.B. Berry, K.I. Booker-Milburn, Practical flow reactor for continuous organic photochemistry, The Journal of Organic Chemistry 70 (19) (2005) 7558–7564.

[14] F. Levesque, P.H. Seeberger, Highly efficient continuous flow reactions using singlet oxygen as a green reagent, Organic Letters 13 (19) (2011) 5008–5011.

[15] R.C.R. Wootton, R. Fortt, A.J. de Mello, A microfabricated nanoreactor for safe, continuous generation and use of singlet oxygen, Organic Process Research and Development 6 (2002) 187–189.

[16] E.E. Coyle, M. Oelgemöller, Micro-photochemistry: photochemistry in microstructured reactors. The new photochemistry of the future? Photochemical and Photobiological Sciences 7 (2008) 1313–1322.

[17] M. Oelgemöller, Highligths of photochemical reactions in microflow reactors, Chemical Engineering Technology 35 (2012) 1–10.

[18] O. Shvydkiv, A. Yavorskyy, S.B. Tan, K. Nolan, N. Hoffmann, A. Youssef, M. Oelgemöller, Microphotochemistry: a reactor comparison study using the photosensitized addition of isopropanol to furanones as a model reaction, Photochemical and Photobiological Sciences 10 (2011) 1399.

[19] W.J. Geldenhuys, S.F. Malan, T. Murugesan, C.J. Van der Schyf, J.R. Bloomquist, Synthesis and biological evaluation of pentacyclo[5.4.0.0^{2,6}.0^{3,10}.0^{5,9}]undecane derivatives as potential therapeutic agents in Parkinson's disease, Bioorganic and Medicinal Chemistry 12 (2004) 1799–1806.

[20] L.H.-A. Prins, J.L. du Preez, S. van Dyk, S.F. Malan, Polycyclic cage structures as carrier molecules for neuroprotective non-steroidal anti-inflammatory drugs, European Journal of Medical Chemistry 44 (2009) 2577–2582.

[21] O.K. Onajole, K. Govender, P. Govender, P.D. ven Helden, H.G. Kruger, G.E.M. Maguire, K. Muthusamy, M. Pillay, I. Wiid, T. Govender, Pentacyclo-undecane derived cyclic tetra-amines: synthesis and evaluation as potent anti-tuberculosis agents, European Journal of Medical Chemistry 44 (2009) 4297–4305.

[22] A.P. Marchand, R.W. Allen, Improved synthesis of pentacyclo [5.4.0.0^{2,6}.0^{3,10}.0^{5,9}]undecane, Journal of Organic Chemistry 39 (11) (1974) 1596.

[23] R.H. Feehs, US Patent 3(554), (1971) 887.

[24] A.E. Cassano, C.A. Martin, R.J. Brandi, O.M. Alfano, Photoreactor analysis and design: fundamentals and applications, Industrial and Engineering Chemistry Research 34 (7) (1995) 2155–2201.

[25] C.A. Martín, M.A. Baltanás, A.E. Cassano, Photocatalytic reactors. II. Quantum efficiencies allowing for scattering effects. An experimental approximation, Journal of Photochemistry and Photobiology A-Chemistry 94 (1996) 173–189.

[26] L. Tessé, J.M. Lamet, Radiative transfer modeling developed at Onera for numerical simulations of reactive flows, The Onera Journal Aerospace Lab 2 (2011).

[27] H.A. Irazoqui, J. Cerdá, A.E. Cassano, The radiation field for the point and line source approximation and the three-dimensional source models: applications to photoreactions, Chemical Engineering Journal 11 (1976) 27–37.

[28] C.S. Zalazar, M.D. Labas, C.A. Martín, R.J. Brandi, O.M. Alfano, A.E. Cassano, The extended use of actinometry in the interpretation of photochemical reaction engineering data, Chemical Engineering Journal 109 (2005) 67.

[29] J.F. Cornet, C.G. Dussap, J.B. Gros, Simplified monodimensional approach for modeling coupling between radiant light transfer and growth kinetics in photo bioreactors, Chemical Engineering Science 50 (1995) 1489–1500.

[30] A.E. Cassano, P.L. Silveston, J.M. Smith, Photochemical reaction engineering, Industrial and Engineering Chemistry 59 (1) (1967) 18–38.